

Jet quenching in pp and pA collisions *

B.G. Zakharov¹

¹*L.D. Landau Institute for Theoretical Physics, GSP-1, 117940, Kosygina Str. 2, 117334 Moscow, Russia*

We study jet quenching in pp and pA collisions in the scenario with formation of a mini quark-gluon plasma. We find a significant suppression effect. For light hadrons at $p_T \sim 10$ GeV we obtained the reduction of the spectra by $\sim [20-30, 25-35, 30-40]\%$ in pp collisions at $\sqrt{s} = [0.2, 2.76, 7]$ TeV. We discuss how jet quenching in pp collisions may change the predictions for the nuclear modification factors in AA collisions for light and heavy flavors. We also give predictions for modification of the photon-tagged and inclusive jet fragmentation functions in high multiplicity pp events.

PACS numbers:

I. INTRODUCTION

One of the manifestation of the quark-gluon plasma (QGP) formation in AA collisions is the jet quenching phenomenon which is dominated by the radiative parton energy loss [1–7]. It leads to suppression of the high- p_T spectra, which is characterized by the nuclear modification factor R_{AA} given by the ratio of the inclusive cross section for AA collisions to the binary-scaled inclusive cross section for pp collisions

$$R_{AA} = \frac{d\sigma(AA \rightarrow hX)/d\mathbf{p}_T dy}{N_{bin} d\sigma(pp \rightarrow hX)/d\mathbf{p}_T dy}. \quad (1)$$

It would be extremely interesting to observe jet quenching in pp and pA collisions, since it would be a direct signal of the mini-QGP formation. The QGP formation in pp and pA collisions have been addressed in several publications recently [8–10] from the viewpoint of the hydrodynamical flow effects. In recent papers [11, 12] we studied the possible manifestations of jet quenching in pp collisions within the light-cone path integral approach [3], which we previously used for analysis of jet quenching in AA collisions [13–16]. In [11] we discussed the medium modification of the γ -tagged fragmentation functions (FFs) and in [12] the medium modification factor R_{pp} and its effect on the nuclear modification factors R_{AA} and R_{pA} . The medium modification factor R_{pp} characterizes the difference between the real inclusive pp cross section, accounting for the final-state jet interaction in the QGP, and the perturbative one, i.e.,

$$d\sigma(pp \rightarrow hX)/d\mathbf{p}_T dy = R_{pp} d\sigma_{pert}(pp \rightarrow hX)/d\mathbf{p}_T dy. \quad (2)$$

Since we cannot switch off the final state interaction in the QGP, the R_{pp} is not an observable quantity. Nevertheless, it may affect the theoretical predictions for R_{AA} . Indeed, in the scenario with the QGP formation in pp collisions one should use in the denominator in (1) the real inclusive pp cross section which differs from the perturbative one. In this case one should compare with experimental R_{AA} the following quantity:

$$R_{AA} = R_{AA}^{st}/R_{pp}, \quad (3)$$

where R_{AA}^{st} is the standard nuclear modification factor calculated using the pQCD predictions for the particle spectrum in pp collisions. The effect of the R_{pp} may be important for the centrality dependence of R_{AA} and the azimuthal anisotropy (simply because in the scenario with the QGP formation in pp collisions α_s becomes bigger). It should also be important for the jet flavor tomography of the QGP [15–18]. Because the effect of R_{pp} on R_{AA} for heavy quarks should be smaller due to weaker jet quenching for heavy quarks in pp collisions. In this talk I review the results of [11, 12] and extend the analysis [12] to heavy flavors.

* Talk at XIth Quark Confinement and the Hadron Spectrum, Saint-Petersburg, Russia, 8-12 September 2014.

II. MINI-QGP IN PROTON-PROTON COLLISIONS

We describe the mini-QGP fireball within 1+1D Bjorken's model [19], which gives $T_0^3\tau_0 = T^3\tau$. For $\tau < \tau_0$ we assume that the medium density $\propto \tau$. As in our previous analyses of jet quenching in AA collisions [13–16], in the basic variant we take $\tau_0 = 0.5$ fm. For the QGP in AA collisions with the lifetime/size $L \gg \tau_0$ the medium effects are not very sensitive to variation of τ_0 . But this may be untrue for pp collisions when the plasma size is considerably smaller. To understand the sensitivity of R_{pp} to τ_0 we also perform calculations for $\tau_0 = 0.8$ fm. To simplify the computations we neglect variation of the initial temperature T_0 with the transverse coordinates. We fix T_0 using the entropy/multiplicity ratio $C = dS/dy / dN_{ch}/d\eta \approx 7.67$ obtained in [20]. The initial entropy density can be written as

$$s_0 = \frac{C}{\tau_0 \pi R_f^2} \frac{dN_{ch}}{d\eta}, \quad (4)$$

where R_f is the fireball radius. We ignore the azimuthal anisotropy, and regard R_f as an effective mini-QGP radius, which includes pp collisions in the whole range of the impact parameter. This approximation seems to be plausible since the jet production should be dominated by the nearly head-on collisions for which the azimuthal effects should be weak.

In jet quenching calculations for the multiplicity density in (4) one should use the multiplicity density of the soft (underlying-event (UE)) hadrons, which is bigger than the minimum bias multiplicity density by a factor (K_{ue}) of ~ 2 [21]. Experimental studies [21–25] show that the UE multiplicity grows with momentum of the leading charged jet hadron at $p_T \lesssim 3-5$ GeV and then flattens out. The plateau region corresponds approximately to $E_{jet} \gtrsim 15-20$ GeV. To fix the $dN_{ch}/d\eta$ in (4) at $\sqrt{s} = 0.2$ TeV we use the UE enhancement factor K_{ue} from PHENIX [22] obtained by dihadron correlation method. Taking for minimum bias non-diffractive events $dN_{ch}^{mb}/d\eta = 2.98 \pm 0.34$ from STAR data [26], we obtained for the UEs in the plateau region $dN_{ch}/d\eta \approx 6.5$. To evaluate the UE multiplicity at $\sqrt{s} = 2.76$ and 5.02 TeV we use the data from ATLAS [23] at $\sqrt{s} = 0.9$ and 7 TeV that give in the plateau region $dN_{ch}/d\eta \approx 7.5$ and 13.9. Assuming that $dN_{ch}/d\eta \propto s^\delta$, by interpolating between $\sqrt{s} = 0.9$ TeV and 7 TeV we obtained for the UE multiplicity density in the plateau region $dN_{ch}/d\eta \approx 10.5$ and 12.6 at $\sqrt{s} = 2.76$ and 5.02 TeV, respectively. We use for R_f the values obtained in numerical simulations of pp collisions at $\sqrt{s} = 7$ TeV performed in [10] within the IP-Glasma model [27]. In [10] it has been found that R_f grows approximately as linear function of $(dN_g/dy)^{1/3}$ and then flattens out (a convenient parametrization of R_f from [10] has been given in [28]). The plateau region corresponds to nearly head-on collisions where the fluctuations of multiplicity are dominated by the fluctuations of the glasma color fields [10]. With the help of the formula for R_f from [28] for the above values of the UE multiplicity densities in the plateau regions we obtain (we take $dN_g/dy = \kappa dN_{ch}/d\eta$ with $\kappa = C45/2\pi^4\xi(3) \approx 2.13$)

$$R_f[\sqrt{s} = 0.2, 2.76, 5.02, 7 \text{ TeV}] \approx [1.3, 1.44, 1.49, 1.51] \text{ fm}. \quad (5)$$

We neglect possible variation of the R_f from RHIC to LHC since our results are not very sensitive to R_f . Using (4) and the ideal gas formula $s = (32/45 + 7N_f/15)T^3$ (with $N_f = 2.5$), we obtain the initial temperatures of the QGP

$$T_0[\sqrt{s} = 0.2, 2.76, 5.02, 7 \text{ TeV}] \approx [199, 217, 226, 232] \text{ MeV}. \quad (6)$$

One sees that the values of T_0 lie well above the deconfinement temperature $T_c \approx 160-170$ MeV.

For initial temperatures (6) the purely plasma phase may exist up to $\tau_{QGP} \sim 1-1.5$ fm. At $\tau > \tau_{QGP}$ the hot QCD matter will evolve in the mixed phase up to $\tau_{max} \sim 2R_f$ where the transverse expansion should lead to fast cooling of the fireball. For $\tau_{QGP} < \tau < \tau_{max}$ the QGP fraction in the mixed phase is approximately $\propto 1/\tau$ [19], and for this reason we can use $1/\tau$ dependence of the number density of the scattering centers in the whole range of τ (but with the Debye mass defined for $T \approx T_c$ at $\tau > \tau_{QGP}$).

The central question for the scenario with mini-QGP formation is the extend to which the mini-fireball created in pp collisions may be treated as a continuous macroscopic medium. This question at present is still open. The lattice studies support the idea that a collective medium may be created in pp collisions. Indeed, the macroscopic behavior of the fireball is possible when the Knudsen number $Kn \sim \tau_c/\tau$ is small. We estimated Kn using the recent lattice results [29] on the electric conductivity σ of the QGP.

From the Drude formula (for massless partons)

$$\sigma \sim \frac{\langle e_q^2 \rangle n_{q+\bar{q}} \tau_c}{3T} \quad (7)$$

and lattice σ from [29] we obtained approximately for the temperatures given in (6) $Kn(\text{quark}) \sim 1$ at $\tau \sim 0.5$ fm and $Kn(\text{quark}) \sim 0.25$ at $\tau \sim 1$ fm. The gluon Knudsen number should be smaller by a factor of $\sim C_F/C_A = 4/9$. This qualitative analysis shows that the collective behavior of the mini-fireball does not seem to be unrealistic. Of course, the inequality $Kn \ll 1$ is just a necessary condition for the hydrodynamic behavior of the QGP. But it cannot guarantee that the QGP is produced quickly after pp collision.

III. MEDIUM INDUCED GLUON SPECTRUM AND PARAMETERS OF THE MODEL

As in [13], we evaluate the medium induced gluon spectrum dP/dx ($x = \omega/E$ is the gluon fractional momentum) for the QGP modeled by a system of the static Debye screened color centers [1]. We use the Debye mass obtained in the lattice analysis [30] giving μ_D/T slowly decreasing with T ($\mu_D/T \approx 3.2$ at $T \sim T_c$, $\mu_D/T \approx 2.4$ at $T \sim 4T_c$). For the plasma quasiparticle masses of light quarks and gluon we take $m_q = 300$ and $m_g = 400$ MeV supported by the analysis of the lattice data [31]. Our results are not very sensitive to m_g , and practically insensitive to the value of m_q . For gluon emission from a quark (or gluon) the x -spectrum may be written [32] through the light-cone wave function of the $gq\bar{q}$ (or ggg) system in the coordinate ρ -representation. Its z -dependence is governed by a two-dimensional Schrödinger equation with the “mass” $\mu = x(1-x)E$ (E is the initial parton energy) in which the longitudinal coordinate z plays the role of time and the potential $v(\rho)$ is proportional to the QGP density/entropy times a linear combination of the dipole cross sections $\sigma(\rho)$, $\sigma((1-x)\rho)$ and $\sigma(x\rho)$. We perform calculations with running α_s frozen at some value α_s^{fr} at low momenta. For gluon emission in vacuum a reasonable choice is $\alpha_s^{fr} \sim 0.7 - 0.8$ [33, 34]. In plasma thermal effects can suppress α_s^{fr} . However, the uncertainties of jet quenching calculations are large and the extrapolation from the vacuum gluon emission to the induced radiation may be unreliable. For this reason we treat α_s^{fr} as a free parameter of the model. In [16] we have observed that data on R_{AA} are consistent with $\alpha_s^{fr} \sim 0.5$ for RHIC and $\alpha_s^{fr} \sim 0.4$ for LHC. The reduction of α_s^{fr} from RHIC to LHC may be due to stronger thermal effects at LHC where the initial temperature is bigger. But the analysis [16] is performed ignoring the medium suppression in pp collisions. Accounting for R_{pp} should increase α_s^{fr} . However, in [16] we used the plasma density vanishing at $\tau < \tau_0$, whereas now we use the QGP density $\propto \tau$, which leads to somewhat stronger medium suppression. As a result, preferable α_s^{fr} (from the standpoint of the description of R_{AA}) remains approximately the same, or a bit larger, as obtained in [16]. If the difference between α_s^{fr} for AA collisions at RHIC and LHC is really due to the thermal effects, then for the mini-QGP with T_0 as given in (6) a reasonable window is $\alpha_s^{fr} \sim 0.6 - 0.7$. In principle for the mini-QGP the thermal reduction of α_s may be smaller than for the large-size plasma (at the same temperature). Because for the mini-QGP a considerable contribution to the induced gluon emission comes from the product of the emission amplitude and complex conjugate one when one of them has the gluon emission vertex outside the medium and is not affected by the medium effects. We perform the calculations for $\alpha_s^{fr} = 0.5, 0.6$ and 0.7 . Note that R_{pp} should be less sensitive to α_s^{fr} than R_{AA} since the typical virtualities for induced gluon emission in the mini-QGP are larger than that in the large-size QGP (see below).

The physical pattern of induced gluon emission in the mini-QGP differs somewhat from that for the large-size QGP. For the mini-QGP when the typical path length in the medium $L \sim 1 - 1.5$ fm the energy loss is dominated by gluons with $L_f \gtrsim L$, where $L_f \sim 2\omega/m_g^2$ is the gluon formation length in the low density limit. In this regime the dominating contribution comes from the $N = 1$ rescattering, and the finite-size and Coulomb effects play a crucial role [35, 36] (see also [37]). On the contrary, for the QGP in AA collisions the induced energy loss is dominated by gluons with $L_f \lesssim L$. Indeed, $L_f \sim 2\omega S_{LPM}/m_g^2$, where S_{LPM} is the LPM suppression factor. For RHIC and LHC typically $S_{LPM} \sim 0.3 - 0.5$ for $\omega \sim 2$ GeV, it gives $L_f \sim 1.5 - 2.5$ fm which is smaller than the typical L for the QGP in AA collisions. In this regime the finite-size effects are much less important and the gluon spectrum is (locally) approximately similar to that in an infinite extent matter. It is important that the induced gluon emission in the mini-QGP is more perturbative than in the large-size QGP. Indeed, from the Schrödinger diffusion relation one can obtain for the typical transverse size of the three parton system $\rho^2 \sim 2\xi/\omega$, where ξ is the path

length after gluon emission. Then, using the fact that $\sigma(\rho)$ is dominated by the t -channel gluon exchanges with virtualities up to $Q^2 \sim 10/\rho^2$ [38] we obtain $Q^2 \sim 5\omega/\xi$. For $\omega \sim 2$ and $\xi \sim 0.5 - 1$ fm it gives $Q^2 \sim 2 - 4$ GeV². The virtuality scale in the gluon emission vertex has a similar form but smaller by a factor of ~ 2.5 [39]. The $1/\xi$ dependence of Q^2 persists up to $\xi \sim L_f$. For the large-size QGP one should replace ξ by the real in-medium L_f (which contains S_{LPM}) which is by a factor of ~ 2 larger than the typical values of ξ for the mini-QGP. It results in a factor of ~ 2 smaller virtualities in AA collisions.

IV. ENERGY LOSS IN THE MINI-QGP

In Fig. 1 we show the energy dependence of the total (radiative plus collisional) and collisional energy loss for partons produced in the center of the mini-QGP fireball for $\alpha_s^{fr} = 0.6$ (as in [39], both the radiative and collisional contributions are defined for the lost energy smaller than half of the initial parton energy). We present results for the fireball parameters obtained for the jet energy dependent UE $dN_{ch}/d\eta$ and for that in the plateau region (details see in [12]). One can see that the energy loss for these two versions (solid and long-dashed lines) become very close to each other at $E \gtrsim 10$ GeV. Our results show that at $E \sim 10 - 20$ GeV for gluons the total energy loss is $\sim 10 - 15\%$ of the initial energy. The contribution of the collisional mechanism is relatively small. The energy loss for the mini-QGP is smaller than that for the large-size QGP in AA collisions obtained in [16] by a factor of ~ 4 .

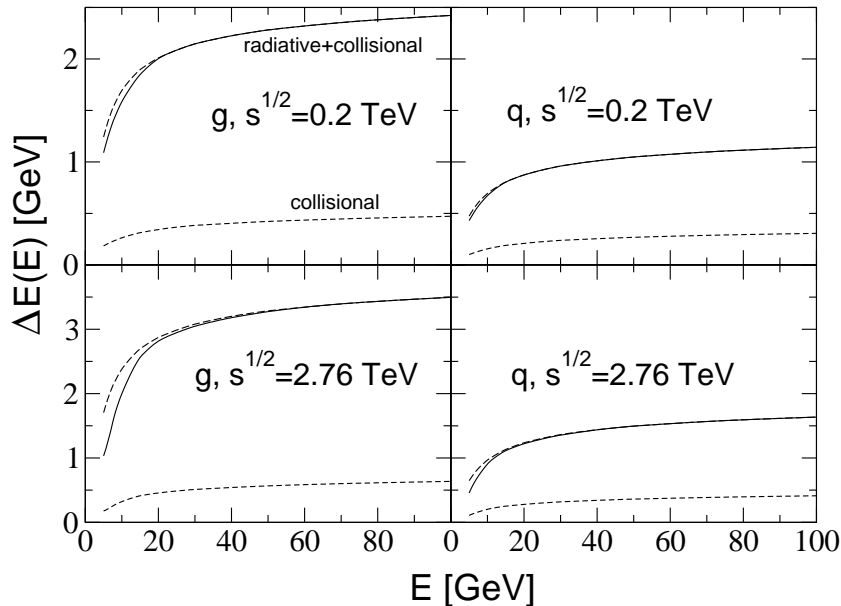


FIG. 1: Energy dependence of the energy loss of gluons (left) and light quarks (right) produced in the center of the mini-QGP fireball at $\sqrt{s} = 0.2$ TeV (upper panels) and $\sqrt{s} = 2.76$ TeV (lower panels). Solid line: total (radiative plus collisional) energy loss calculated with the fireball radius R_f and the initial temperature T_0 obtained with the UE $dN_{ch}/d\eta$ dependent on the initial parton energy E ; dashed line: same as solid line but for collisional energy loss; long-dashed line: same as solid line but for R_f and T_0 obtained with the UE $dN_{ch}/d\eta$ in the plateau region as given by (5) and (6). All the curves are for $\alpha_s^{fr} = 0.6$.

In Fig. 2 we show the the radiative and collisional gluon energy loss vs the path length L for $E = 20$ and 50 GeV for $T_0 = 199$ and 217 MeV, corresponding to $\sqrt{s} = 0.2$ and 2.76 TeV. To illustrate the difference between pp and AA collisions we present also predictions for radiative energy loss for $T_0 = 320$ MeV corresponding to central $Au + Au$ collisions at $\sqrt{s} = 0.2$ TeV, and for $T_0 = 420$ MeV corresponding to central $Pb + Pb$ collisions at $\sqrt{s} = 2.76$ TeV. We rescaled the predictions for AA collisions by the factor $(T_0(pp)/T_0(AA))^3$. One sees that at $L \geq \tau_0$ the radiative energy loss is approximately a linear function of L , and at $L < \tau_0$ the radiative energy loss is approximately $\propto L^3$ (since the leading $N = 1$ rescattering term to the effective Bethe-Heitler cross section is $\propto L$ [35, 36] and integration over the longitudinal coordinate of the scattering center gives additional two powers of L). From comparison of the radiative

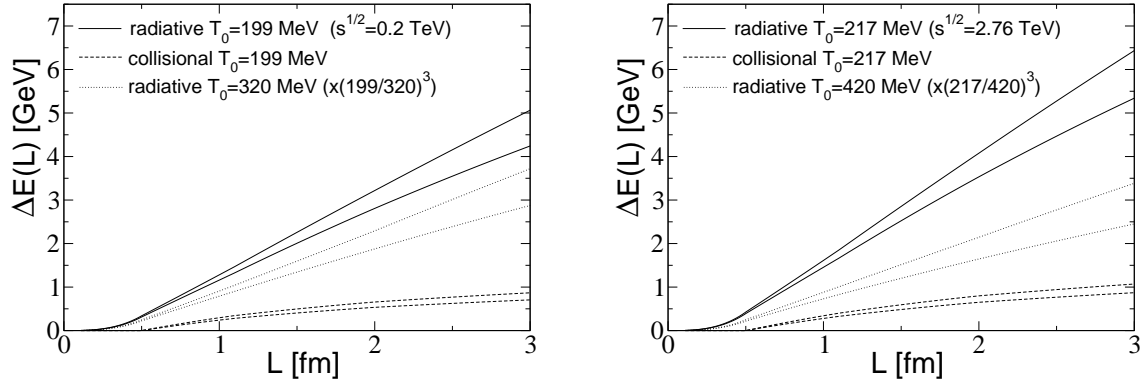


FIG. 2: Left: Radiative (solid) and collisional (dashed) gluon energy loss vs the path length L in the QGP with $T_0 = 199$ MeV for (bottom to top) $E = 20$ and 50 GeV. The dotted lines show radiative energy loss for $T_0 = 320$ MeV rescaled by the factor $(199/320)^3$. All curves are calculated for $\alpha_s^{fr} = 0.6$. Right: same as in the left figure but for $T_0 = 217$ and 420 MeV and the rescaling factor $(217/420)^3$ for dotted lines.

energy loss for $T_0 = 199$ and 217 MeV to that for $T_0 = 320$ and 420 MeV one can see a deviation from the T^3 scaling by factors of ~ 1.5 and ~ 2 , respectively. This difference persists even at $L \sim 1$ fm. It comes mostly from the increase of the LPM suppression (and partly from the increase of the Debye mass) for the QGP produced in AA collisions.

V. MEDIUM MODIFICATION OF THE INCLUSIVE SPECTRA

A. Perturbative and medium modified inclusive cross sections

As usual we write the perturbative inclusive cross section in (2) in terms of the vacuum parton \rightarrow hadron FF $D_{h/i}$

$$\frac{d\sigma_{pert}(pp \rightarrow hX)}{d\mathbf{p}_T dy} = \sum_i \int_0^1 \frac{dz}{z^2} D_{h/i}(z, Q) \frac{d\sigma(pp \rightarrow iX)}{d\mathbf{p}_T^i dy}, \quad (8)$$

where $d\sigma(pp \rightarrow iX)/d\mathbf{p}_T^i dy$ is the ordinary hard cross section, $\mathbf{p}_T^i = \mathbf{p}_T/z$ is the parton transverse momentum. We write the real inclusive cross section in a similar form but with the medium modified FF $D_{h/i}^m$

$$\frac{d\sigma(pp \rightarrow hX)}{d\mathbf{p}_T dy} = \sum_i \int_0^1 \frac{dz}{z^2} D_{h/i}^m(z, Q) \frac{d\sigma(pp \rightarrow iX)}{d\mathbf{p}_T^i dy}. \quad (9)$$

Here it is implicit that $D_{h/i}^m$ is averaged over the geometry of the parton process and over the impact parameter of pp collision.

We calculated the hard cross sections in the LO pQCD with the CTEQ6 [40] parton distribution functions (PDFs). To simulate the higher order effects we calculate the partonic cross sections for the virtuality scale of $\alpha_s cQ$ with $c = 0.265$ as in the PYTHIA event generator [41]. For the hard scale Q in the FFs in (8), (9) we use p_T/z . We calculate the vacuum FFs $D_{h/j}$ as a convolution of the KKP [42] parton \rightarrow hadron FFs at soft scale $Q_0 = 2$ GeV with the DGLAP parton \rightarrow parton FFs $D_{j/i}^{DGLAP}$ describing the evolution from Q to Q_0 . The latter have been computed with the help of PYTHIA [41]. The medium modified FFs $D_{j/i}^m$ have been calculated in a similar way but inserting between the DGLAP parton \rightarrow parton FFs and the KKP parton \rightarrow hadron FFs the parton \rightarrow parton FFs $D_{j/i}^{ind}$ which correspond to the induced radiation stage in the QGP. The $D_{j/i}^{ind}$ have been calculated from the medium induced gluon spectrum using Landau's method [43] imposing the flavor and momentum conservation (see [13]

for details). Note that the permutation of the DGLAP and the induced stages gives a very small effect [13].

Since we ignore the azimuthal effects, the averaging of the medium modified FFs over the geometrical variables of the hard parton process and over the impact parameter of pp collision is simply reduced to averaging over the parton path length L in the QGP. We have performed averaging over L for the distribution of hard processes in the impact parameter plane obtained with the quark distribution from the MIT bag model (we assume that the valence quarks and the hard gluons radiated by the valence quarks have approximately the same distribution in the transverse spacial coordinates). We obtained that practically in the full range of the pp impact parameter the distribution in L is sharply peaked around $L \approx \sqrt{S_{ov}/\pi}$ (here S_{ov} is the overlap area for two colliding bags). It shows that R_f at the same time gives the typical path length for fast partons. We found that, as compared to $L = R_f$, the L -fluctuations reduce the medium modification by only $\sim 10 - 15\%$.

We treat the collisional energy loss, which is relatively small [39], as a small perturbation to the radiative mechanism, and incorporate it simply by renormalizing the QGP temperature in calculating the medium modified FFs for the induced radiation (see [13] for details).

B. Predictions for R_{pp}

In Fig. 3 we present the results for R_{pp} of charged hadrons at $\sqrt{s} = 0.2, 2.76$ and 7 TeV for $\alpha_s^{fr} = 0.5, 0.6$ and 0.7 . To illustrate the sensitivity of the results to τ_0 we show the curves for $\tau_0 = 0.5$ and 0.8 fm. The suppression effect for the basic variant with $\tau_0 = 0.5$ fm turns out to be quite large at $p_T \lesssim 20$ GeV both for RHIC and LHC. One can see that for $\tau_0 = 0.8$ fm the reduction of the suppression is not very significant. Fig. 3 shows that, as we expected, R_{pp} does not exhibit a strong dependence on α_s^{fr} . Although the plasma density is smaller at $\sqrt{s} = 0.2$ TeV, the suppression effect is approximately similar to that at $\sqrt{s} = 2.76$ and 7 TeV. It is due to a steeper slope of the hard cross sections at $\sqrt{s} = 0.2$ TeV. The increase in the suppression from $\sqrt{s} = 2.76$ to $\sqrt{s} = 7$ TeV is relatively small. In the left part of Fig. 4 we show a comparison between R_{pp} at $\sqrt{s} = 7$ TeV for the minimum bias and the UE $dN_{ch}/d\eta$. One can see that even the minimum bias $dN_{ch}/d\eta$ gives a considerable suppression. The right part of Fig. 4 shows variation of R_{pp} between $\sqrt{s} = 7$ and 100 TeV. One sees that the energy dependence of R_{pp} is weak.

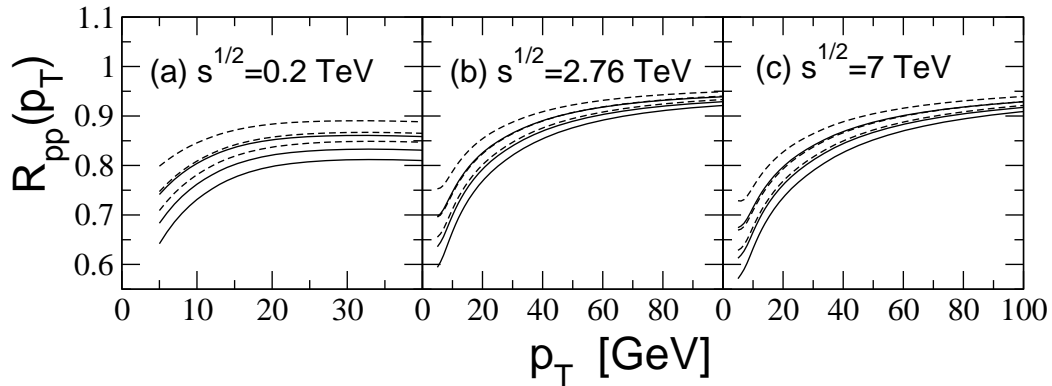


FIG. 3: R_{pp} of charged hadrons at $\sqrt{s} = 0.2$ (a), 2.76 (b), 7 (c) TeV for (top to bottom) $\alpha_s^{fr} = 0.5, 0.6$ and 0.7 for $\tau_0 = 0.5$ (solid) and 0.8 (dashed) fm.

To study the sensitivity of R_{pp} to the fireball radius we also performed the calculations for R_f given by (5) times 0.7 and 1.3 . We found that in these two cases the medium suppression is smaller by $\sim 3\%$ and 10% , respectively. The weak dependence on R_f is due to a compensation between the enhancement of the energy loss caused by increase of the fireball size and its suppression due to reduction of the QGP density. Note that the stability of R_{pp} against variations of R_f shows that the variation of the plasma density in the transverse coordinates should not be very important. Indeed, the gluon spectrum is dominated by $N = 1$ rescattering term which is a linear functional of the plasma density profile along the fast parton trajectory. Therefore the energy loss for a more realistic plasma density (with a higher density

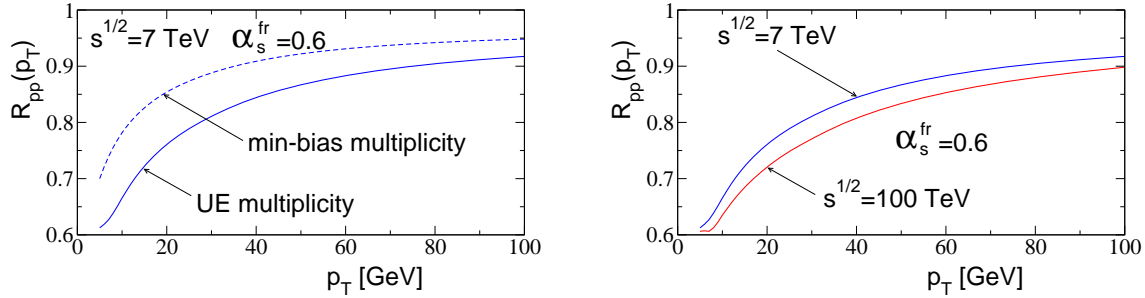


FIG. 4: Left: R_{pp} of charged hadrons at $\sqrt{s} = 7$ TeV for the UE (solid line) and minimum bias (dashed line) $dN_{ch}/d\eta$. Right: R_{pp} of charged hadrons at $\sqrt{s} = 7$ TeV (blue) and $\sqrt{s} = 100$ TeV (red) for UE $dN_{ch}/d\eta$.

in the central region) can be roughly approximated by a linear superposition of that for the step density distributions with different R_f . And it should not change strongly R_{pp} as compared to our calculations.

Fig. 3 shows the results for the typical UE multiplicity density. An accurate accounting for the fluctuations of the UE $dN_{ch}/d\eta$ is impossible since it should be done on the event-by-event basis, and requires detailed information about dynamics of the UEs. To understand how the event-by-event fluctuations of the UE $dN_{ch}/d\eta$ may change our results, we evaluated R_{pp} assuming that the distribution in the UE $dN_{ch}/d\eta$ is the same at each impact parameter and jet production point. We used the distribution in $dN_{ch}/d\eta$ from CMS [24] measured at $\sqrt{s} = 0.9$ and 7 TeV. It satisfies approximately KNO scaling similar to that in minimum bias events [44]. For this reason one can expect that it can be used for RHIC conditions as well. We observed that the fluctuating $dN_{ch}/d\eta$ suppresses $(1 - R_{pp})$ by only $\sim 5 - 6\%$ both for RHIC and LHC energies. This says that our approximation without the event-by-event fluctuations of the QGP parameters should be good.

C. Effect of R_{pp} on R_{AA}

To illustrate the effect of the mini-QGP in pp collisions on R_{AA} in Fig. 5 we compare our results for R_{AA} with the data for π^0 -mesons in central $Au + Au$ collisions at $\sqrt{s} = 0.2$ TeV (a) from PHENIX [45], and with the data for charged hadrons in central $Pb + Pb$ collisions at $\sqrt{s} = 2.76$ TeV (b,c) from ALICE [46] and CMS [47]. We show the predictions for R_{AA} defined by (3) with (red) the $1/R_{pp}$

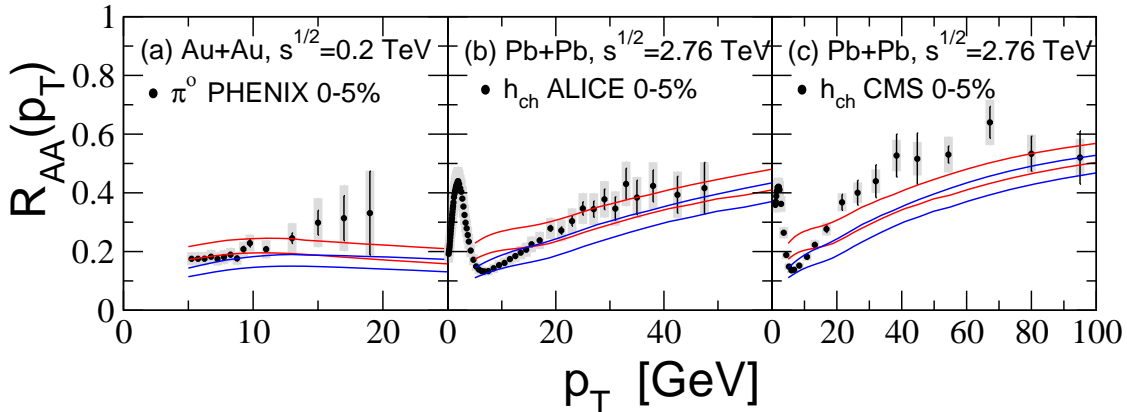


FIG. 5: (a) R_{AA} of π^0 for 0-5% central $Au + Au$ collisions at $\sqrt{s} = 0.2$ TeV from our calculations for (top to bottom) $\alpha_s^{fr} = 0.5$ and 0.6 with (red) and without (blue) $1/R_{pp}$ factor in (3). (b,c) R_{AA} for charged hadrons for 0-5% central $Pb + Pb$ collisions at $\sqrt{s} = 2.76$ TeV from our calculations for (top to bottom) $\alpha_s^{fr} = 0.4$ and 0.5 with (red) and without (blue) $1/R_{pp}$ factor in (3). The red curves are obtained with the factor $1/R_{pp}$ calculated with $\alpha_s^{fr} = 0.6$. Data points are from PHENIX [45] (a), ALICE [46] (b) and CMS [47] (c). Systematic experimental errors are shown as shaded areas.

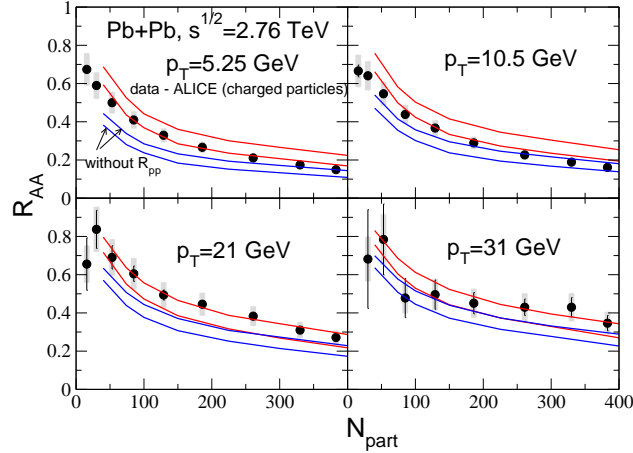


FIG. 6: R_{AA} of charged particles vs N_{part} for $Pb + Pb$ at $\sqrt{s} = 2.76$ TeV with (red) and without (blue) R_{pp} , for (top to bottom) $\alpha_s^{fr} = 0.4$ and 0.5 for $\sqrt{s} = 2.76$ TeV, R_{pp} is calculated at $\alpha_s^{fr} = 0.6$. Data points are from ALICE [52].

factor, and for R_{AA}^{st} without (blue) this factor. We use the R_{pp} for $\alpha_s^{fr} = 0.6$. We calculated R_{AA}^{st} for $\alpha_s^{fr} = 0.5$ and 0.6 at $\sqrt{s} = 0.2$ TeV, and for $\alpha_s^{fr} = 0.4$ and 0.5 at $\sqrt{s} = 2.76$ TeV. Because these values give better agreement with the data. We accounted for the nuclear modification of the PDFs with the EKS98 correction [48]. As in [16], we take $T_0 = 320$ MeV for central $Au + Au$ collisions at $\sqrt{s} = 0.2$ TeV, and $T_0 = 420$ MeV for central $Pb + Pb$ collisions at $\sqrt{s} = 2.76$ TeV obtained from hadron multiplicity pseudorapidity density $dN_{ch}/d\eta$ from RHIC [49] and LHC [50, 51]. At $p_T \sim 10$ GeV for RHIC the agreement of the theoretical R_{AA} (with the $1/R_{pp}$ factor) with the data is somewhat better for $\alpha_s^{fr} = 0.6$, and for LHC the value $\alpha_s^{fr} = 0.5$ seems to be preferred by the data. The agreement in the p_T -dependence of R_{AA} is not perfect (especially for LHC). The theory somewhat underestimates the slope of the data. It seems that the regions of large p_T support $\alpha_s^{fr} = 0.5$ and 0.4 for RHIC and LHC, respectively. The inclusion of R_{pp} even reduces a little the slope of R_{AA} . However, it does not seem to be very dramatic since the theoretical uncertainties may be significant.

Fig. 5 shows that the effect of R_{pp} on R_{AA} in central AA collisions can approximately be imitated by a simple reduction of α_s^{fr} . However, it is clear that R_{pp} may be important for the azimuthal effects and the centrality dependence of R_{AA} since in the scenario with the mini-QGP formation in pp collisions the values of α_s^{fr} become bigger. The effect of R_{pp} on the centrality dependence of R_{AA} is shown Fig. 6. R_{pp} can also affect the flavor dependence of R_{AA} since the suppression effect for heavy quarks in pp collisions is smaller. It is illustrated in Figs. 7–9 for the p_T -dependence of the ratio of the R_{AA} for heavy and light flavors. One sees that at $p_T \gtrsim 10$ GeV R_{pp} reduces the difference between the nuclear suppression of the

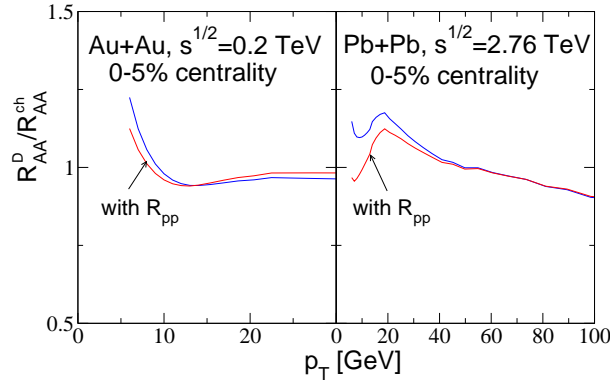


FIG. 7: Effect of R_{pp} due to mini-QGP on ratio R_{AA} for D -mesons to R_{AA} for light charged hadrons. $\alpha_s^{fr} = 0.6$ for $\sqrt{s} = 0.2$ TeV and $\alpha_s^{fr} = 0.5$ for $\sqrt{s} = 2.76$ TeV, R_{pp} for light and heavy flavors is calculated at $\alpha_s^{fr} = 0.6$.

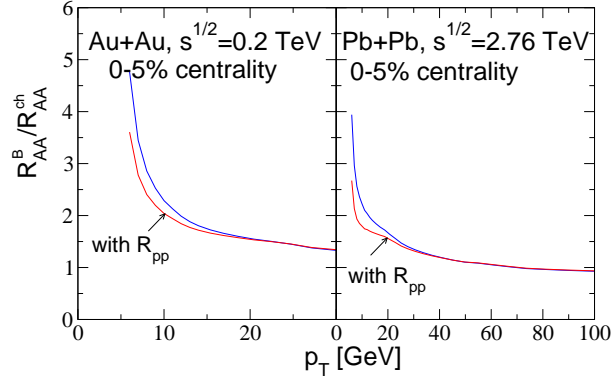


FIG. 8: Effect of R_{pp} due to mini-QGP on ratio R_{AA} for B -mesons to R_{AA} for light charged hadrons. $\alpha_s^{fr} = 0.6$ for $\sqrt{s} = 0.2$ TeV and $\alpha_s^{fr} = 0.5$ for $\sqrt{s} = 2.76$ TeV, R_{pp} for light and heavy flavors is calculated at $\alpha_s^{fr} = 0.6$.

spectra for heavy and light flavors. In Fig. 10 we show the effect of R_{pp} on the centrality dependence of R_{AA} for D -mesons. One can see that R_{pp} may improve somewhat agreement with the data.

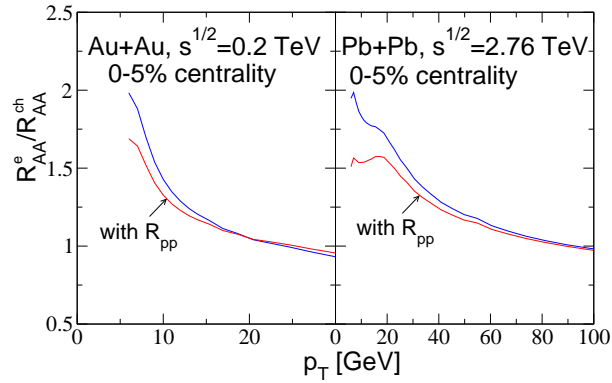


FIG. 9: Effect of R_{pp} due to mini-QGP on ratio R_{AA} for non-photonic electrons to R_{AA} for light charged hadrons. $\alpha_s^{fr} = 0.6$ for $\sqrt{s} = 0.2$ TeV and $\alpha_s^{fr} = 0.5$ for $\sqrt{s} = 2.76$ TeV, R_{pp} for light and heavy flavors is calculated at $\alpha_s^{fr} = 0.6$.

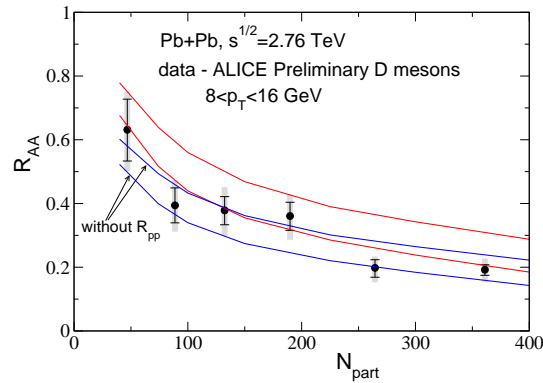


FIG. 10: R_{AA} of D -mesons vs N_{part} for $Pb + Pb$ at $\sqrt{s} = 2.76$ TeV with (red) and without (blue) R_{pp} , for (top to bottom) $\alpha_s^{fr} = 0.4$ and $\alpha_s^{fr} = 0.5$, R_{pp} is calculated at $\alpha_s^{fr} = 0.6$. Data points are from ALICE [53].

D. Jet quenching in pA collisions

In the scenario with the QGP production in pp collisions the correct formula for R_{pA} reads $R_{pA} = R_{pA}^{st}/R_{pp}$. Evidently, the sizes and the initial temperatures of the plasma fireballs in pp and pA collisions should not differ strongly. For this reason for R_{pA} the uncertainties related to variation of α_s (or the temperature dependence of the QGP density and the Debye mass) are smaller than for R_{AA} . The ALICE data [54] show a small deviation from unity of R_{pPb} at $\sqrt{s} = 5.02$ TeV at $p_T \gtrsim 10$ GeV, where the Cronin effect should be weak. In the scenario with the QGP formation this is possible only if the magnitudes of the medium suppression in pp and pPb collisions are close to each other. Unfortunately, presently the UE multiplicity in pPb collisions is unknown. But it is clear that it cannot be smaller than the minimum bias multiplicity density $dN_{ch}^{mb}/d\eta = 16.81 \pm 0.71$ [55]. In order to understand the acceptable range of the UE multiplicity density in pPb collisions in the scenario with the mini-QGP formation we calculated R_{pPb} for $dN_{ch}/d\eta = K_{ue}dN_{ch}^{mb}/d\eta$ for $K_{ue} = 1, 1.25, \text{ and } 1.5$.

In our calculations as a basic choice we use the parametrization of $R_f(pPb)$ vs the multiplicity given in [28] obtained from the results of simulation of the pPb collisions performed in [10] within the IP-Glasma model [27]. Ref. [27] gives $R_f(pPb)$ that is close to $R_f(pp)$ where $R_f(pp) \propto (dN_g/dy)^{1/3}$, but $R_f(pPb)$ flattens at higher values of the gluon density. Using formula (4), we obtained for $K_{ue} = [1, 1.25, 1.5]$

$$R_f(pPb) \approx [1.63, 1.88, 1.98] \text{ fm}, \quad (10)$$

$$T_0(pPb) \approx [222, 229, 235] \text{ MeV}. \quad (11)$$

Fig. 11 shows comparison of our results with the data on R_{pPb} at $\sqrt{s} = 5.02$ TeV from ALICE [54]. To illustrate the sensitivity to $R_f(pPb)$ we also present the results for $R_f(pPb)$ 1.2 and 1.4 times greater. We show the curves with (red) and without (blue) the $1/R_{pp}$ factor. As for AA case we account for the nuclear modification of the PDFs with the EKS98 correction [48]. It gives a small deviation of R_{pPb} from unity even without parton energy loss. The results for R_{pp} are also shown (green). All the curves are obtained with $\alpha_{fr} = 0.6$. However, our predictions for R_{pPb} (with the $1/R_{pp}$ factor) are quite stable against variation of α_s^{fr} since the medium effects are very similar for pp and pPb collisions.

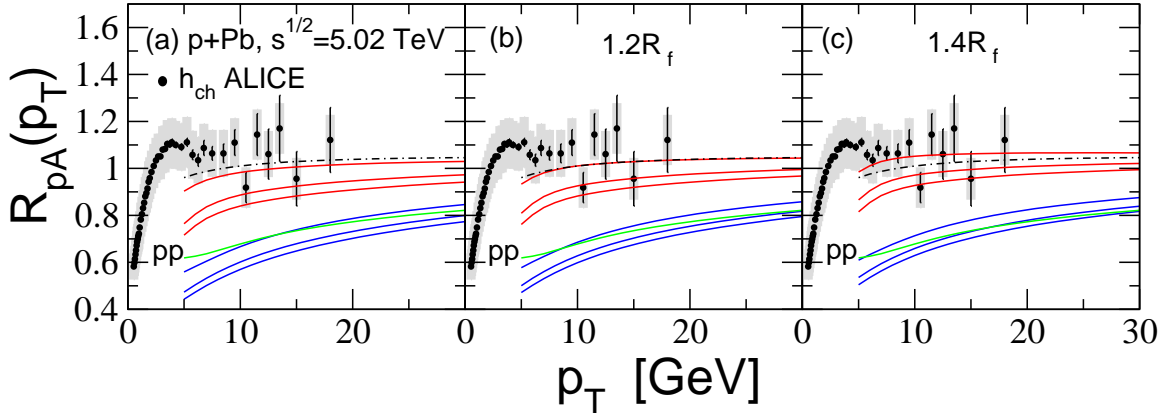


FIG. 11: (a) R_{pPb} for charged hadrons at $\sqrt{s} = 5.02$ TeV from our calculations for $\alpha_s^{fr} = 0.6$ with (red) and without (blue) the $1/R_{pp}$ factor for (top to bottom) $K_{ue} = 1, 1.25$ and 1.5 for the $R_f(pPb)$ from (10). (b,c) same as (a) but for $R_f(pPb)$ times 1.2 and 1.4. The green line shows R_{pp} . The dot-dashed line shows R_{pPb} due to the EKS98 correction [48] to the nucleus PDFs. Data points are from ALICE [54].

Fig. 11 shows that at $p_T \gtrsim 10$ GeV, where the Cronin effect should be small, our predictions (with $1/R_{pp}$ factor) obtained with $K_{ue} = 1$ agree qualitatively with the data. The agreement becomes better for larger $R_f(pPb)$. But just as for R_{pp} the variation of R_{pPb} with the fireball size is relatively weak. The curves for the higher UE multiplicities ($K_{ue} = 1.25$ and 1.5) lie below the data. Thus we see that the data from ALICE [54] may be consistent with the formation of the QGP in pp and pPb collisions if the UE multiplicity is close to the minimum bias one. This condition may be weakened if the size of the

fireball in pPb collisions is considerably bigger than predicted in [10]. But the physical picture may change if we take into account the meson-baryon Fock component in the proton. Indeed, in pA collisions the final-state interaction may be smaller due to meson-baryon Fock component in the proton. The weight of the MB -component may be as large as $\sim 40\%$ [56]. Contrary to pp case in pA collisions practically in all events meson should produce its own fireball. It means that in $\sim 40\%$ events an asymmetric two-fireball configuration may be produced (as illustrated in the left part of Fig. 12). Since jet may propagate without interaction with one of the fireball (typically it is the meson fireball as shown in the right part of Fig. 12), the final-state interaction should be weaker than for a symmetric fireball (for same $dN_{ch}/d\eta$). Note that the two-fireball state naturally generates the azimuthal flow for the soft particles as well.

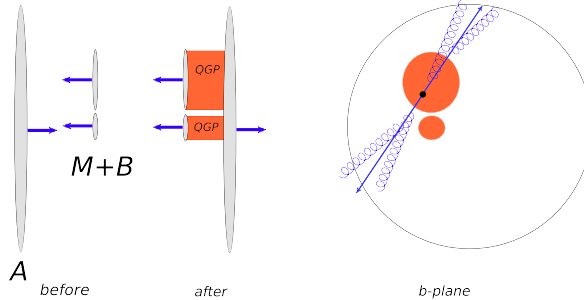


FIG. 12: A cartoon of the production of a two-fireball state in pA collisions from the meson-baryon Fock component of the proton (a); A cartoon of the jet quenching for the two-fireball state (b)

VI. MEDIUM MODIFICATION OF PHOTON-TAGGED AND INCLUSIVE JETS IN HIGH-MULTIPLICITY PROTON-PROTON COLLISIONS

For a direct observation of the medium effects in pp collisions one can use measurement of the jet FF in γ +jet events for different UE multiplicities. To understand the prospects of this method we evaluate the medium modification of the γ -tagged FF at $\sqrt{s} = 7$ TeV at $y = 0$. The values of the R_f and T_0 for different values of $dN_{ch}/d\eta$ obtained using (4) are given in Table I. For $dN_{ch}/d\eta \gtrsim 40$ we obtain T_0 which is about that for central $Au + Au$ collisions at RHIC.

TABLE I: R_f and T_0 for different $dN_{ch}/d\eta$.

$dN_{ch}/d\eta$	3	6	20	40	60
R_f (fm)	1.046	1.27	1.538	1.538	1.538
T_0 (MeV)	177	196	258	325	372

In γ +jet events the energy of the hard parton, E_T , in the direction opposite to the tagged photon is smeared around the photon energy, E_T^γ . But using the results of the NLO calculations [57] one can show that at $E_T^\gamma \gtrsim 25$ GeV and $z \lesssim 0.9$ the smearing can be safely neglected (for details, see [11]). To be conservative we present results for $z < 0.8$, where the effect of smearing is practically negligible and one can set $E_T = E_T^\gamma$. Then, as in [58], we can write the γ -tagged FF as a function of the UE multiplicity density $dN_{ch}/d\eta$ (for clarity we denote it by N) as

$$D_h(z, E_T^\gamma, N) = \left\langle \left\langle \sum_i r_i(E_T^\gamma) D_{h/i}^m(z, E_T^\gamma, N) \right\rangle \right\rangle, \quad (12)$$

where, as in (9), $D_{h/i}^m$ is the medium modified FF for $i \rightarrow h$ process, and r_i is the fraction of the $\gamma + i$ parton state in the γ +jet events, $\langle \dots \rangle$ means averaging over the transverse geometrical variables of pp collision and jet production, which includes averaging over the fast parton path length L in the QGP.

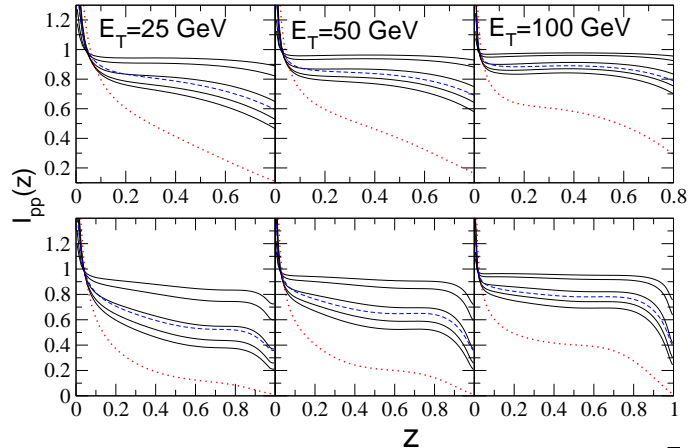


FIG. 13: I_{pp} for γ -tagged (upper panels) and inclusive (lower panels) jet FFs at $\sqrt{s} = 7$ TeV for $dN_{ch}/d\eta = [3, 6, 20, 40, 60]$ (solid line). The order (top to bottom) of the curves at large z corresponds to increasing values of $dN_{ch}/d\eta$. The dashed blue line shows ratio of the FFs for $dN_{ch}/d\eta = 40$ and 3. The red dotted line shows the medium modification factor at $\sqrt{s} = 2.76$ TeV for the QGP with $T_0 = 420$ MeV and $L = 5$ fm for $\alpha_s^{fr} = 0.4$.

Just as for R_{pp} we have performed averaging over L using the distribution of hard processes in the impact parameter plane obtained with the quark distribution from the MIT bag model. As compared to $L = R_f$ the L -fluctuations reduce the medium modification by $\sim 10 - 15\%$. In Fig. 13 we present the results for the medium modification factor (for charged hadrons)

$$I_{pp}(z, E_T, N) = D_h(z, E_T, N) / D_h^{vac}(z, E_T) \quad (13)$$

for the γ -tagged (upper panels) jets for $E_T = [25, 50, 100]$ GeV at $\sqrt{s} = 7$ TeV. For comparison we also show the results for inclusive (lower panels) jets. The smearing effect is irrelevant to inclusive jets and we show the results for the whole range of z . For illustration of the difference between pp and AA collisions we also present the curves for $\sqrt{s} = 2.76$ TeV for $L = 5$ fm and $T_0 = 420$ MeV that can be regarded as reasonable values for $Pb + Pb$ collisions (we used $\alpha_s^{fr} = 0.4$, which is favored by the data on $R_{AA}(p_T)$ at $p_T \gtrsim 20$ GeV). Fig. 13 shows that there is a considerable quenching effect for $dN_{ch}/d\eta \gtrsim 20$. Note that the observed strong quenching of inclusive jets is qualitatively supported by the preliminary data from ALICE [59] that indicate that for the high multiplicity UEs jets undergo a softer fragmentation.

Since the vacuum FFs are unobservable, in practice, to observe the medium effect one should simply compare the FFs for different multiplicities. In Fig. 13 we show the ratio of the FFs for $N = 40$ and $N = 3$ (for inclusive jets this ratio cannot be measured, and we show it just to illustrate the difference in magnitudes of the effect for γ -tagged and inclusive jets). As for R_{pp} we have investigated the sensitivity of our results to variation of R_f , and found that I_{pp} is quite stable against variation of R_f .

VII. SUMMARY

Assuming that a mini-QGP fireball may be created in pp collisions, we have evaluated the medium modification of high- p_T particle spectra for light and heavy flavors and medium modification factors for the γ -triggered and inclusive jet FFs. For $p_T \sim 10$ GeV we obtained $R_{pp} \sim [0.7 - 0.8, 0.65 - 0.75, 0.6 - 0.7]$ at $\sqrt{s} = [0.2, 2.76, 7]$ TeV. We have studied the effect of R_{pp} on the theoretical predictions for the nuclear modification factor R_{AA} in AA collisions at RHIC and LHC energies. We found that R_{pp} does not change dramatically the description of the data on R_{AA} for light hadrons in central AA collisions, and its effect may be imitated by some renormalization of α_s . But inclusion of R_{pp} changes the centrality dependence of R_{AA} . Also, R_{pp} weakens the flavor dependence of R_{AA} .

Our results show that the ALICE data [54] on R_{pPb} may be consistent with the scenario with the QGP formation if in pPb collisions the UE multiplicity is close to the minimum bias one. But this condition may be weakened due to presence in the proton wave function of the meson-baryon Fock component. We leave analysis of its effect for future work.

We demonstrated that in pp collisions with UE multiplicity density $dN_{ch}/d\eta \sim 20 - 40$ the mini-QGP can suppress the γ -triggered FF at $E_T \sim 25 - 100$ GeV and $z \sim 0.5 - 0.8$ by $\sim 10 - 40\%$, and for inclusive jets the effect is even stronger.

Acknowledgments

I would like to thank P. Arnold for the invitation to give this talk at this XIth Quark Confinement and the Hadron Spectrum International Conference. This work is supported in part by the grant RFBR 12-02-00063-a and the program SS-6501.2010.2.

-
- [1] M. Gyulassy and X.N. Wang, Nucl. Phys. **B420**, 583 (1994).
 - [2] R. Baier, Y.L. Dokshitzer, A.H. Mueller, S. Peigné, and D. Schiff, Nucl. Phys. **B483**, 291 (1997); *ibid.* **B484**, 265 (1997).
 - [3] B.G. Zakharov, JETP Lett. **63**, 952 (1996); *ibid* **65**, 615 (1997); **70**, 176 (1999); Phys. Atom. Nucl. **61**, 838 (1998).
 - [4] R. Baier, D. Schiff, and B.G. Zakharov, Ann. Rev. Nucl. Part. **50**, 37 (2000).
 - [5] U.A. Wiedemann, Nucl. Phys. **A690**, 731 (2001).
 - [6] M. Gyulassy, P. Lévai, and I. Vitev, Nucl. Phys. **B594**, 371 (2001).
 - [7] P. Arnold, G.D. Moore, and L.G. Yaffe, JHEP **0206**, 030 (2002).
 - [8] P. Bozek, Acta Phys. Polon. **B41**, 837 (2010).
 - [9] J. Casalderrey-Solana and U.A. Wiedemann, Phys. Rev. Lett. **104**, 102301 (2010).
 - [10] A. Bzdak, B. Schenke, P. Tribedy, and R. Venugopalan, arXiv:1304.3403.
 - [11] B.G. Zakharov, Phys. Rev. Lett. **112**, 032301 (2014).
 - [12] B.G. Zakharov, J. Phys. **G41**, 075008 (2014).
 - [13] B.G. Zakharov, JETP Lett. **88**, 781 (2008).
 - [14] B.G. Zakharov, JETP Lett. **93**, 683 (2011).
 - [15] B.G. Zakharov, JETP Lett. **96**, 616 (2013).
 - [16] B.G. Zakharov, J. Phys. **G40**, 085003 (2013).
 - [17] N. Armesto, M. Cacciari, A. Dainese, C.A. Salgado, and U.A. Wiedemann, Phys. Lett. **B637**, 362 (2006).
 - [18] A. Buzzatti and M. Gyulassy, Phys. Rev. Lett. **108**, 022301 (2012).
 - [19] J.D. Bjorken, Phys. Rev. **D27**, 140 (1983).
 - [20] B. Müller and K. Rajagopal, Eur. Phys. J. **C43**, 15 (2005).
 - [21] A.A. Affolder *et al.* [CDF Collaboration], Phys. Rev. **D65**, 092002 (2002).
 - [22] J. Jia, for the PHENIX Collaboration, contribution to the Quark Matter 2009 Conf., March 30 - April 4, Knoxville, Tennessee; arXiv:0906.3776.
 - [23] G. Aad *et al.* [ATLAS Collaboration], Phys. Rev. **D83**, 112001 (2011).
 - [24] S. Chatrchyan *et al.* [CMS Collaboration], JHEP **1109**, 109 (2011).
 - [25] B. Abelev *et al.* [ALICE Collaboration] JHEP **1207**, 116 (2012).
 - [26] B.I. Abelev *et al.* [STAR Collaboration], Phys. Rev. **C79**, 034909 (2009).
 - [27] B. Schenke, P. Tribedy, and R. Venugopalan, Phys. Rev. Lett. **108**, 252301 (2012).
 - [28] L. McLerran, M. Praszalowicz, and B. Schenke, arXiv:1306.2350.
 - [29] A. Amato, G. Aarts, C. Allton, P. Giudice, S. Hands, and J.-I. Skullerud, arXiv:1310.7466.
 - [30] O. Kaczmarek and F. Zantow, Phys. Rev. **D71**, 114510 (2005).
 - [31] P. Lévai and U. Heinz, Phys. Rev. **C57**, 1879 (1998).
 - [32] B.G. Zakharov, JETP Lett. **80**, 617 (2004).
 - [33] N.N. Nikolaev and B.G. Zakharov, Phys. Lett. **B327**, 149 (1994).
 - [34] Yu.L. Dokshitzer, V.A. Khoze, and S.I. Troyan, Phys. Rev. **D53**, 89 (1996).
 - [35] B.G. Zakharov, JETP Lett. **73**, 49 (2001).
 - [36] P. Aurenche and B.G. Zakharov, JETP Lett. **90**, 237 (2009) [arXiv:0907.1918].
 - [37] P. Arnold, Phys. Rev. **D80**, 025004 (2009).
 - [38] N.N. Nikolaev and B.G. Zakharov, Phys. Lett. **B332**, 184 (1994).
 - [39] B.G. Zakharov, JETP Lett. **86**, 444 (2007).
 - [40] S. Kretzer, H.L. Lai, F. Olness, and W.K. Tung, Phys. Rev. **D69**, 114005 (2004).
 - [41] T. Sjostrand, L. Lonnblad, S. Mrenna, and P. Skands, arXiv:hep-ph/0308153.
 - [42] B.A. Kniehl, G. Kramer, and B. Potter, Nucl. Phys. **B582**, 514 (2000).
 - [43] R. Baier, Yu.L. Dokshitzer, A.H. Mueller, and D. Schiff, JHEP **0109**, 033 (2001).

- [44] A. Dumitru and E. Petreska, arXiv:1209.4105.
- [45] A. Adare *et al.* [PHENIX Collaboration], arXiv:1208.2254.
- [46] B. Abelev *et al.* [ALICE Collaboration], Phys. Lett. **B720**, 52 (2013).
- [47] S. Chatrchyan *et al.* [CMS Collaboration], Eur. Phys. J. **C72**, 1945 (2012).
- [48] K.J. Eskola, V.J. Kolhinen, and C.A. Salgado, Eur. Phys. J. **C9**, 61 (1999).
- [49] B.I. Abelev *et al.* [STAR Collaboration], Phys. Rev. **C79**, 034909 (2009).
- [50] S. Chatrchyan *et al.* [CMS Collaboration], JHEP **1108**, 141 (2011).
- [51] K. Aamodt *et al.* [ALICE Collaboration], Phys. Rev. Lett. **106**, 032301 (2011).
- [52] B. Abelev *et al.* [ALICE Collaboration], Phys. Lett. **B720**, 52 (2013).
- [53] E. Bruna, for the ALICE Collaboration, contribution to 14th International Conference on Strangeness in Quark Matter (SQM2013), J. Phys. Conf. Ser. **509**, 012080 (2014) [arXiv:1401.1698].
- [54] B. Abelev *et al.* [ALICE Collaboration], Phys. Rev. Lett. **110**, 082302 (2013).
- [55] B. Abelev *et al.* [ALICE Collaboration], Phys. Rev. Lett. **110**, 032301 (2013).
- [56] J. Speth, A W. Thomas, Adv. Nucl. Phys. **24**, 83 (1997).
- [57] H. Zhang, J.F. Owens, E. Wang, and X.-N. Wang, Phys. Rev. Lett. **103**, 032302 (2009).
- [58] X.-N. Wang, Z. Huang, and I. Sarcevic, Phys. Rev. Lett. **77**, 231 (1996).
- [59] H.L. Vargas, for the ALICE Collaboration, J. Phys. Conf. Ser. **389**, 012004 (2012) [arXiv:1208.0940].
- [60] B. Abelev *et al.* [ALICE Collaboration], Phys. Rev. Lett. **110**, 082302 (2013).